Applied Magnetic Resonance (2023) 54:1423–1443
https://doi.org/10.1007/s00723-023-01607-x

Applied
Magnetic Resonance

ORIGINAL PAPER

Quantifying Liquid-Solid Mass Transfer in a Trickle Bed Using $T_2 - T_2$ Relaxation Exchange NMR

Scott V. Elgersma[1] · Qingyuan Zheng[1] · Nikolaos Avrantinis[1] · Andrew J. Sederman[1] · Michael D. Mantle[1] · Lynn F. Gladden[1]

Received: 15 June 2023 / Revised: 14 August 2023 / Accepted: 19 August 2023 /
Published online: 11 September 2023

Abstract

Measurement of the liquid-solid mass transfer coefficient within a trickle bed (i.e. gas-liquid flow within a packed bed) of porous silica pellets is achieved through the use of $T_2 - T_2$ relaxation exchange nuclear magnetic resonance (NMR). Compared to many conventional measurement techniques, the NMR method enables measurement of mass transport using pellets of real commercial interest. Mass transfer coefficients measured using the NMR technique over a range of liquid Reynolds number, $0.2 \leq Re_L \leq 1.4$, are compared to a number of literature correlations, with values measured using the NMR method falling within the range predicted by the correlations. The results demonstrate the importance of considering both the flow conditions and the type of pellets used to develop mass transport correlations in trickle beds. This novel NMR application may be utilized in the future to screen catalyst pellets in trickle beds for optimal mass transport properties.

1 Introduction

Trickle bed reactors are used in many industrial processes where gas-liquid-solid contact is required, including hydrodesulpherization, hydrocracking, selective oxidation reactions, and Fischer-Tropsch synthesis [1–3]. In a trickle bed reactor, solid catalyst pellets are packed randomly into a tube; gas and liquid are then passed through the packing in co-current downflow. The flow physics in trickle beds is complex, being a function of the bed structure, gas-liquid hydrodynamics, and gas-liquid-solid surface interactions. The performance of trickle bed reactors

Prepared for Applied Magnetic Resonance issue on the occasion of Bernhard Blümich's 70th birthday.

✉ Lynn F. Gladden
lfg1@cam.ac.uk

[1] Magnetic Resonance Research Centre, Department of Chemical Engineering & Biotechnology, University of Cambridge, Philippa Fawcett Drive, Cambridge CB3 0AS, UK

is intrinsically linked to these complex hydrodynamics, which dictate the heat and mass transport in the bed. External mass transfer from the inter-pellet liquid phase to the catalyst pellet surface often limits the performance of trickle bed reactors [4–6].

In trickle beds, the liquid-solid mass transfer coefficient, k, (herein simply referred to as the mass transfer coefficient) is a proportionality constant linking the driving force for mass transfer (typically the concentration difference) and the mass transport flux between the inter-pellet liquid and pellet surface [3, 7]. For an arbitrary species (denoted A), the rate of mass transfer between the bulk inter-pellet liquid and the pellet surface is written as:

$$F_A = \eta k a_S \left(C_A^{\text{inter}} - C_A^S\right), \tag{1}$$

where $C_A^{\text{inter}} - C_A^S$, is the concentration difference between the bulk inter-pellet liquid and surface, a_S is the external surface area per unit volume of inter-pellet void space in the bed, η is the pellet wetting efficiency defined as the fraction of the external pellet surface covered in liquid, and F_A is the resulting rate of mass transfer per unit volume of inter-pellet void space in the bed. Due to the similar effect η and k have on the overall rate of mass transfer, and because they are difficult to measure separately, it is common to group these parameters together as ηk when quantifying the mass transport in trickle beds.

The mass transfer coefficient is a complex function of the diffusive and advective transport within trickle beds. Numerous techniques have been developed to measure the mass transfer coefficient including the dissolution method [8, 9], the electrochemical method [10, 11] and the ion-exchange method [12]. However, these methods require the use of a model analogue bed (e.g. a solid metallic electrode pellet in the case of the electrochemical method) rather than the porous catalyst pellets of relevance to trickle bed reactors. The ability to measure the mass transfer coefficient using the catalyst pellets of commercial interest is especially important for trickle beds, as pellet wettability and porosity are known to affect the hydrodynamics in trickle beds [13, 14]. To measure the mass transfer coefficient on the catalyst pellets of interest, in situ techniques have been developed whereby a trickle bed reactor is operated and the reactor conversion data are fit to a model to determine k [15, 16]. Whilst this enables one to study the pellets of interest, a clear disadvantage of these in situ methods is the need to assume a reaction kinetics model and subsequently model the entire reactor to extract k from the data. Alternatively, the dynamic adsorption method [17] can be used for studying mass transport in beds of porous pellets, however, the results can be influenced by the effect of dispersion and complex transient models must be used to interpret the results and extract the mass transfer coefficient. Utilizing magnetic resonance imaging (MRI), Zheng et al. [4] were the first to develop a truly *operando* technique for measuring the mass transfer coefficient in an operating trickle bed reactor. Whilst this original approach allows the mass transfer coefficient to be directly quantified in an operating reactor, it assumes that intra-pellet (internal) transport resistance is negligible and requires expertise in state-of-the-art MRI methods and data analysis. Clearly, to optimize the mass transport properties for the catalyst and reactor technology used at

scale, a method for non-invasively measuring mass transport at the pellet-scale in beds of real catalyst pellets is highly desirable.

Recently, Elgersma et al. [18] developed a technique for measuring the mass transfer coefficient for single phase flow in a bed of catalyst support pellets using $T_2 - T_2$ relaxation exchange NMR. $T_2 - T_2$ relaxation exchange NMR, first developed by Lee et al. [19], has been extensively utilized to probe molecular exchange between different relaxation environments in systems ranging from cement to articular cartilage [20–28]. Cross-peaks (often termed off-diagonal peaks) in the 2D $T_2 - T_2$ exchange map are indicative of molecular exchange between different relaxation environments. When the exchanging environments have the same T_1 relaxation times, and the exchange process is slow compared to T_2 relaxation, the cross-peaks can be interpreted quantitatively as the fraction of molecules exchanging during a given exchange time, t_{mix}. In real systems, these assumptions often break down and the effects of fast exchange and T_1 relaxation hinder the quantitative interpretation of $T_2 - T_2$ exchange data. Blümich and co-workers have made significant progress in the quantitative analysis of $T_2 - T_2$ relaxation exchange data. In particular, rather than only consider the effect of molecular exchange, Blümich et al. introduced a framework for directly modelling the $T_2 - T_2$ exchange experiment as a magnetization transport problem [29]. In this framework, the effects of T_1 relaxation and fast exchange are directly accounted for, and by fitting simulated $T_2 - T_2$ datasets to experimental results, it is possible to obtain quantitative measurements of molecular exchange. This magnetization transport framework was then further extended to advection-diffusion problems by using the Bloch-Torrey equations to describe $T_2 - T_2$ relaxation exchange for single phase flow in a packed bed [30]. Motivated by the magnetization transport framework approach, Elgersma et al. developed a magnetization transport model to quantify the mass transfer coefficient from $T_2 - T_2$ exchange measurements for single phase flow in a packed bed [18].

The objective of the present work is to extend the method developed by Elgersma et al. [18] to measure the mass transfer coefficient in a trickle bed, by adapting the magnetization transport model developed for single phase flow in a packed bed to treat the multiphase flow occurring within a trickle bed. The magnetization transport model requires knowledge of the liquid saturation, β, in the bed, which can be measured using a simple NMR Hahn echo experiment. $T_2 - T_2$ exchange measurements are conducted in a trickle bed of porous silica pellets over a range of liquid flow rates, and the magnetization transport model is subsequently used to extract the mass transfer coefficient, ηk. The resulting mass transfer coefficients are subsequently compared to common correlations in the literature and discussed. The $T_2 - T_2$ exchange method enables the direct measurement of molecular exchange in a trickle bed and offers a relatively straightforward approach to quantify the mass transfer coefficient utilizing the porous catalyst pellets of true commercial relevance.

2 Magnetization Transport Model

The magnetization transport model developed by Elgersma et al. [18] to quantify k from $T_2 - T_2$ exchange measurements for single phase flow in packed beds must be modified for use in the three phase trickle bed (i.e., a gas-liquid flow within a packed

bed). The diffusion equation describing the transport of magnetization within the pellet remains unchanged from that used to describe single-phase flow in a packed bed, and is written [18]:

$$\begin{cases} \frac{\partial M^{\text{intra}}}{\partial t} = D^{\text{intra}} \nabla^2 M^{\text{intra}} - R_{1,2}^{\text{intra}} \left(M^{\text{intra}} - M^{\text{eq}} \right) \\ M^{\text{intra}}(t=0) = M_0^{\text{intra}} \\ \left. \frac{\partial M^{\text{intra}}}{\partial r} \right|_{r=0} = 0 \\ -D^{\text{intra}} \left. \frac{\partial M^{\text{intra}}}{\partial r} \right|_{r=d_p/2} \phi = k \left(M_S^{\text{inter}} - M^{\text{inter}} \right) \end{cases}, \tag{2}$$

where M^{intra} is the intra-pellet magnetization density, M_S^{inter} is the magnetization density at the pellet surface in the inter-pellet phase, M^{inter} is the bulk (well-mixed) magnetization density in the inter-pellet phase, M^{eq} is the thermal equilibrium magnetization density, r is the radial spatial coordinate of the pellet (ranging from $r = 0$ at the pellet centre to $r = d_p/2$ at the outer surface of the pellet), d_p is the pellet diameter, D^{intra} is the intra-pellet molecular diffusion coefficient, $R_{1,2}$ is the relaxation rate, and k is the mass transfer coefficient. Equation (2) describes the intra-pellet magnetization transport. To describe the inter-pellet transport, since the bed is only partially saturated with liquid, the wetting efficiency, η, and the inter-pellet liquid saturation, β, must be introduced. The inter-pellet magnetization density in the bed is then written (modifying Eq. (6) from [18]):

$$\frac{\partial M^{\text{inter}}}{\partial t} = a_S \eta k \left(M_S^{\text{inter}} - M^{\text{inter}} \right) - \frac{Q}{\beta V^{\text{inter}}} M^{\text{inter}} - R_{1,2}^{\text{inter}} \left(M^{\text{inter}} - M^{\text{eq}} \right), \tag{3}$$

where Q is the volumetric flow rate and V^{inter} is the inter-pellet void volume within the active region of the NMR probe. Note that the wetting efficiency, η, is defined as the fraction of external pellet surface area covered in liquid, and the inter-pellet liquid saturation, β, is defined as the ratio of the volume of inter-pellet liquid to the total inter-pellet void volume in the bed. For a packed bed of spherical pellets it is easy to show that the pellet external surface area is $a_S = \frac{6(1-\epsilon)}{d_p \epsilon}$ where ϵ is the voidage of the bed (ratio of inter-pellet void volume to the total volume of the bed). The average magnetization density in the bed, M^{tot}, measured during the NMR acquisition, is written as the volume average of the inter- and intra-pellet magnetization density:

$$M^{\text{tot}} = \frac{\epsilon \beta}{\epsilon \beta + (1-\epsilon)\phi} M^{\text{inter}} + \frac{(1-\epsilon)\phi}{\epsilon \beta + (1-\epsilon)\phi} \overline{M^{\text{intra}}}, \tag{4}$$

where ϕ is the pellet porosity and $\overline{M^{\text{intra}}}$ is the magnetization density averaged across the intra-pellet phase. Thus, the magnetization transport model for $T_2 - T_2$ exchange in a trickle bed becomes Eqs. (2–4) together with the $T_2 - T_2$ exchange relaxation rate scheme, $R_{1,2}^i$, defined in [18]:

$$R^i_{1,2}(t) = \begin{cases} {T_2^i}^{-1}, 0 < t < t_e^A \\ {T_1^i}^{-1}, t_e^A \le t < t_e^A + t_{mix} \\ {T_2^i}^{-1}, t_e^A + t_{mix} \le t < t_e^A + t_{mix} + t_e^B \end{cases}, \quad (5)$$

where i denotes the intra- or inter-pellet phase, t_e^A and t_e^B represent the time spent in the transverse plane during the first and second CPMG encoding intervals, respectively, and t_{mix} is the mixing time. To model the cross-peak evolution during the $T_2 - T_2$ experiment, the algorithm reported in [18] is used. Note that in treating the intra-pellet magnetization transport as a 1D problem (using Eq. (2)), it is implicitly assumed that the pellet wetting is spherically symmetric. In reality, this will not be the case, as the wetting is known to be non-symmetric in trickle beds [31]. However, given that the magnetization transport model was found to be insensitive to the overall wetting fraction, η, for the trickle bed conditions studied herein (as shown in "Model Parameterization" section), this assumption is not considered to quantitatively affect values of the mass transfer coefficient extracted from the model in this work.

2.1 Model Parameterization

In this section, the parameterization of the magnetization transport model, Eq. (2–4), is discussed. The liquid saturation, β, is easily measured from a simple NMR Hahn-echo experiment, as presented in the Results and Discussion, and as such is not used as a fitting parameter in the model but rather a known constant. The parameters $\epsilon, \phi, Q, V^{inter}$, and a_S are determined based on well-established measurement techniques or geometrical arguments. The parameters D^{intra}, T_1^i and T_2^i are measured using standard $D - T_2$ and $T_1 - T_2$ NMR correlation experiments, as discussed in [18]. This leaves η and k as the only unknown parameters in the model.

Since the mass transfer rate in the bed is proportional to ηk (from Eq. (1)), it is sensible to group the parameters in the model as ηk and η. To investigate the effect of the model parameters ηk and η, the magnetization transport model was used to simulate the cross-peak evolution profile, $\frac{I_{XP}}{I_{TP}}\left(t_{mix}\right)$, for a range of values of ηk and η. The cross-peak evolution profiles, simulated by solving Eqs. (2–4) using the algorithm reported in [18], are shown in Fig. 1. The pellet and bed parameters used in these simulations correspond to the trickle bed studied in this work, namely $d_p = 1.3$ mm, $D^{intra} = 1.25 \times 10^{-9}$ m^2 s^{-1}, $\epsilon = 0.39$, $\phi = 0.69$, $T_1^{intra} = 1.2$ s, $T_1^{inter} = 2.7$ s, $T_2^{intra} = 0.15$ s and $T_2^{inter} = 1.2$ s (these parameters are discussed further in the "Data processing and modelling" section and Table 1). Further, the liquid saturation was set as $\beta = 0.48$ and the flow rate was $Q = 0.33$ mL s^{-1} (consistent with the trickle bed studied here at $Re_L = 0.8$). All numerical details regarding the solution of the magnetization transport model are identical to those reported in [18]. From Fig. 1a, it is seen that the cross-peak evolution I_{XP}/I_{TP}, is insensitive to the wetting efficiency, η, at constant $\eta k = 2 \times 10^{-5}$ m s^{-1}. This is because, at low rates of mass transfer (low ηk), external transport limitations dominate, and as such the cross-peak

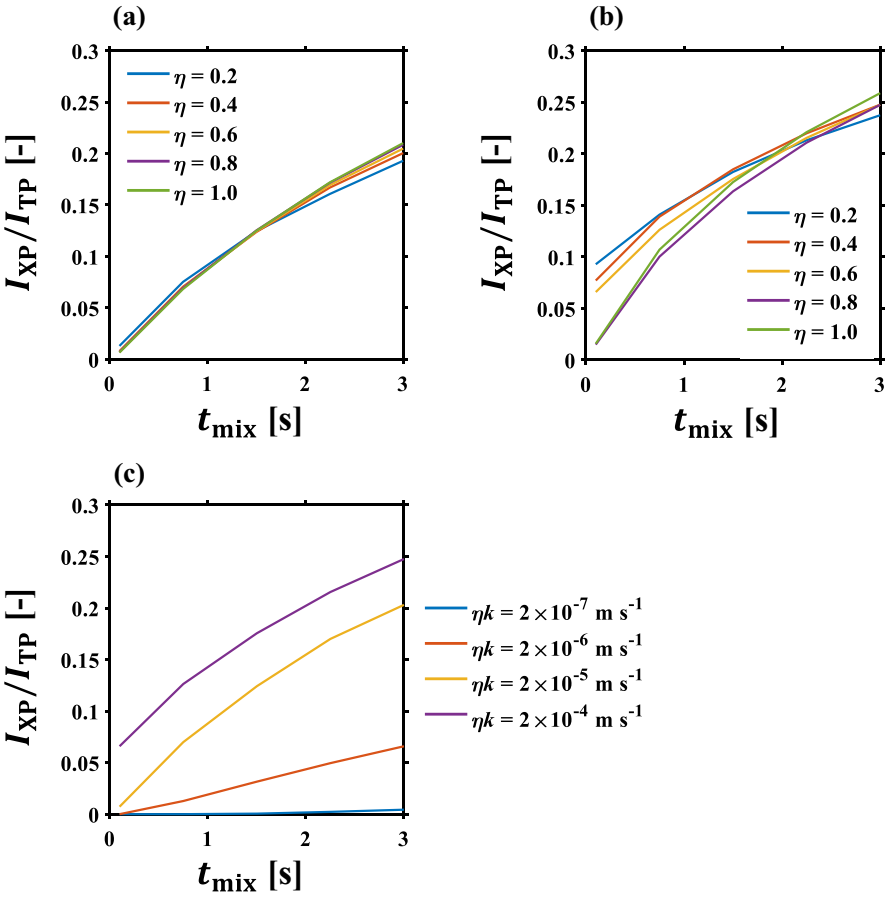

Fig. 1 Sensitivity of cross-peak evolution profile calculated using the magnetization transport model to parameters ηk and k. **a** effect of η at constant $\eta k = 2 \times 10^{-5}$ m s^{-1}; **b** effect of η at constant $\eta k = 2 \times 10^{-4}$ m s^{-1}; **c** effect of ηk at constant $\eta = 0.6$

Table 1 Parameters used in the trickle bed magnetization transport model

Parameter	
d_p [mm]	1.3
$D^{intra} \times 10^9$ [m^2 s^{-1}]	1.25
ϵ [−]	0.39
ϕ [−]	0.69
T_1^{intra} [s]	1.2
T_1^{inter} [s]	2.7
T_2^{intra} [s]	0.15
T_2^{inter} [s]	1.2

evolution is only sensitive to the total rate of transport (which is proportional to ηk). However, at the larger mass transfer rate of $\eta k = 2 \times 10^{-4}$ m s^{-1} where internal diffusion limits the transport, the cross-peak evolution shows some sensitivity towards the wetting efficiency at constant ηk (Fig. 1b). This can be understood by considering Eq. (2) which describes the diffusive transport of magnetization within a pellet. In Eq. (2), k is treated as $\eta k/\eta$ due to the grouping of parameters that is being used here. Thus, at constant ηk, variable η will impact the gradient in magnetization at the pellet boundary which in turn affects the diffusive flux of magnetization. Therefore, when internal diffusion resistance is significant (at high ηk) the cross-peak evolution is dependent on η, as seen in Fig. 1b. At constant η, the cross-peak evolution is very sensitive to ηk, as seen in Fig. 1c, especially in the range of $\eta k = 2 \times 10^{-6}$–$2 \times 10^{-5}$ m s^{-1}. This is highly desirable, as it indicates that ηk can be measured accurately by fitting the magnetization transport model to experimental $T_2 - T_2$ exchange results. In contrast, as the results in Fig. 1a, b show, the model is only sensitive to the effect of η at large values of ηk. Thus at low values of ηk, η should not be interpreted quantitatively and potentially should be set as a fixed parameter to ensure robust model fits. In this work η was set as a constant value, as discussed later in the "Data processing and modelling" section.

3 Materials and Methods

3.1 Materials and Trickle Bed Setup

The experimental setup used to conduct $T_2 - T_2$ exchange experiments within a trickle bed is shown in Fig. 2. A 27 mm inner diameter tube constructed from polyether ether ketone (PEEK) was loaded with porous silica spheres and placed vertically through the bore of a 7.1 T superconducting magnet. The same Q50 silica spheres (Fuji Silysia) used by Elgersma et al. [18] were used as the packing material in this work (mean pore diameter 49.8 nm) with an average pellet diameter d_p = 1.3 mm. During packing, the bed was periodically tapped to consolidate the packing structure, and the entire 1 m length of the bed was packed with silica pellets. Deionized water (Elga PureLab Option DV-25) and air were used as the working fluids for all experiments. Compressed air was stepped down in pressure to 1.2 bara using a regulator valve, and the gas flow was measured and controlled using a variable area flow meter (Brooks Instrument, Sho-Rate 1355) equipped with a needle flow control valve. Liquid was supplied to the trickle bed using a peristaltic pump (Watson Marlow 505S) with a 2 L vessel used at the pump outlet to dampen any flow oscillations and provide steady liquid flow to the trickle bed. Gas and liquid were introduced to the bed using a perforated gas-liquid distributor, details of which are described elsewhere [32]. The portion of the trickle bed within the NMR active region of the spectrometer was approximately 50 cm from the bed inlet, and 40 cm from the bed outlet, ensuring the section studied had no inlet or outlet flow effects. The combined gas-liquid flow exiting the bed was sent to a 10 L glass vessel, where the air was vented to atmosphere and the liquid was recycled to the bed. Liquid flow rate was measured by routing the flow exiting the bed to a volumetric cylinder for

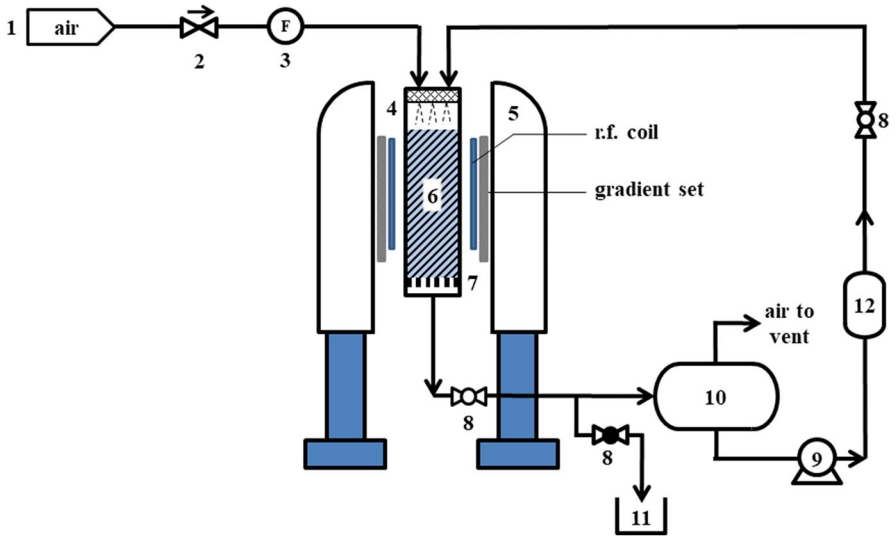

Fig. 2 Schematic of magnetic resonance trickle bed rig used to conduct $T_2 - T_2$ exchange experiments. (1) compressed air supply, (2) regulator valve, (3) variable area flow meter, (4) gas-liquid inlet flow distributor, (5) 7.1 T superconducting magnet (6) 27 mm ID PEEK tube used as trickle bed, (7) gas-liquid outlet flow distributor, (8) stainless steel ball valve, (9) peristaltic pump, (10) 10 L glass vessel for separating liquid and gas, (11) volumetric cylinder for liquid flow rate measurements; (12) 2 L vessel

a known time interval. Stainless steel 1/8″ Swagelok tubing was used to facilitate flow throughout the flow loop, whilst 4 mm silicone rubber tubing was used for the peristaltic pump.

3.2 NMR Experiments

NMR experiments were conducted using a super-wide bore Bruker AV300 7.1 T superconducting magnet equipped with a 3-axis gradient set with maximum gradient strength 0.8 T m^{-1}. A 66 mm diameter birdcage ^{1}H r.f. coil tuned to 300.87 MHz was used for signal excitation and acquisition. The typical duration for a 90° hard pulse was 78 µs.

$T_2 - T_2$ exchange experiments were conducted using the standard pulse sequence shown in [18], consisting of two CPMG echo trains separated by a mixing time during which the magnetization is stored along the z-axis (and subject only to T_1 relaxation). The mixing time, t_{mix}, was varied from 0.1 to 3.0 s in 5 increments to capture the temporal evolution of the cross-peak intensity. The inter-echo spacing was 8 ms and the repetition time was 7.5 s, resulting in an acquisition time of ~ 1.5 h for a single experiment at one t_{mix} value. All other experimental details for the $T_2 - T_2$ exchange experiments were identical to those used in [18].

To measure the total amount of liquid in the bed, from which the total liquid saturation, β, was subsequently calculated, a Hahn echo experiment was conducted using a standard (spatially unresolved) spin echo sequence. An echo time of 1 ms

was used to eliminate any background signal with $T_2 \ll 1$ ms. A spectral width of 100 kHz was used and 32k complex points in the FID were collected. A repetition time of 7.5 s was used, and 8 scans were averaged resulting in a total experiment time of 61 s. At each condition studied, 3 repeat measurements were conducted to ensure repeatability.

3.3 Experimental Conditions

The bed was fully saturated with liquid by closing the bed outlet and feeding liquid to the bed while the gas inlet was open to atmosphere. The bed remained fully flooded for 12 h to give liquid sufficient time to permeate within all pellets and voids in the bed. $T_2 - T_2$ exchange and Hahn echo magnetic resonance experiments were then conducted on the fully flooded bed. The bed outlet was then opened, and the bed was allowed to freely drain under gravity for 1 h. The total liquid in the bed was then measured using the Hahn echo experiment. Following the completion of experiments on the drained bed, gas and liquid flow were introduced to the bed. The flow was allowed to stabilize for 1 h before commencing NMR experiments. Measurements were conducted at four liquid flow rates, $Q =$ 0.07, 0.18, 0.33 and 0.547 mL s^{-1}, beginning with the lowest liquid flow rate first, and successively increasing the liquid flow rate for each condition. As such, the trickle bed was kept in the Levec wetted mode [33, 34] for the entirety of this study. The gas flow was kept constant at 91 NL h^{-1}, giving a gas phase Reynolds number of $Re_G = 3.8$. Note that the gas-phase Reynolds number is defined as $Re_G = \frac{\rho_G u_G d_p}{\mu_G}$, where ρ_G is the gas density, μ_G is the gas viscosity, and u_G is the gas superficial velocity (calculated using the bed diameter). At each flow condition $T_2 - T_2$ exchange and Hahn echo experiments were conducted. All experiments were conducted at 25 ± 3 °C and 1.1 ± 0.05 bara.

3.4 Data Processing and Modelling

Data acquired from Hahn echo experiments were Fourier transformed and the real part of the resulting spectra were 0^{th} and 1^{st} order phase corrected. The spectra were integrated giving the total signal intensity, I, corresponding to liquid water within the bed. The measurements of I were then used to calculate the liquid saturation in the bed, β, details of which follow in the Results and Discussion.

Data acquired from $T_2 - T_2$ exchange measurements were processed as described in Elgersma et al. [18] to obtain the cross-peak evolution, $I_{XP}/I_{TP}(t_{mix})$, at each flow condition studied. To summarize, the acquired 2D magnetization decay data were 0^{th} order phase corrected and the real part of the even echoes was retained. The fast 2D inverse Laplace transform algorithm of Venkataramanan et al. [35] based on singular value decomposition was used to invert the time-domain data and obtain the 2D $T_2 - T_2$ joint probability distribution. The cross-peak intensity, I_{XP}, was then calculated from the 2D $T_2 - T_2$ distribution by integrating the cross-peak regions.

The magnetization transport model for the trickle bed, as given by Eqs. (2–4), was solved numerically to simulate the cross-peak evolution. The numerical scheme

used to solve the model equations was the same as that reported in [18], whereby the method of lines was used to discretize the spatial dimension of the PDE and the resulting system of ODEs was solved. As explained in [18], the 2D magnetization decay was simulated using the transport model with the relaxation rate scheme set to be consistent with the experimental pulse sequence parameters used. The simulated 2D magnetization decay was then used to compute the simulated cross peak intensity by post-processing the simulation data in a manner identical to that used for the experimental data. Because of the insensitivity of the model cross-peak evolution to η at low or intermediate values of ηk (shown in Fig. 1), η was set as a constant value $\eta = 0.5$ and was not used as a fitting parameter. The model was then used to fit the experimentally obtained cross-peak profiles, $I_{XP}/I_{TP}(t_{mix})$, using the Levenberg-Marquardt algorithm with ηk as the sole fitting parameter. Simulations were subsequently conducted at $\eta = 0.2$ and $\eta = 0.8$ and in all cases the resulting best-fit value of ηk varied by $< 5\%$, thereby confirming that fixing the wetting efficiency to $\eta = 0.5$ did not quantitatively impact the best-fit values of ηk. The parameters used in the magnetization transport model are reported in Table 1. The bed voidage, ϵ, was determined using the correlation of Foumeny and Benyahia [36]. The intra-pellet diffusivity, D^{intra}, pellet porosity, ϕ, and the T_1 relaxation times were taken from the values reported for the same silica pellets in [18]. The T_2 intra- and inter-pellet relaxation times used in the model were taken as the log-mean value of the respective peaks obtained from a $T_2 - T_2$ experiment on the fully flooded bed.

4 Results and Discussion

First, the measurement of the liquid saturation in the bed, as required by the magnetization transport model for determining the mass transfer coefficient, is reported using a simple Hahn echo experiment and the results are compared to correlations in the literature. Next, the results from $T_2 - T_2$ exchange, and the subsequent fits of the magnetization model to the data are presented. Finally, the mass transfer coefficients, ηk, extracted from the $T_2 - T_2$ exchange measurements are compared to common mass transfer correlations and discussed.

4.1 Measurement of Liquid Saturation, β

The NMR spectra resulting from the Hahn echo experiment on the fully flooded bed, the fully drained bed ($Re_L = 0$) and the bed under various trickle flow conditions are shown in Fig. 3. Note that the liquid phase Reynolds number is defined as $Re_L = \frac{\rho_L u_L d_p}{\mu_L}$, where ρ_L is the liquid density, μ_L is the liquid viscosity, and u_L is the liquid superficial velocity (calculated using the bed diameter). It is seen that the total signal intensity decreases when the bed is drained, and then increases as the liquid flow rate increases, indicating the total liquid holdup in the bed increases with liquid flow rate as expected [37–39]. Further, the chemical shift of the water in the bed changes slightly when the bed is drained and gas is introduced to the bed, shifting from ~4.8 to ~4.2 ppm, along with broadening of the lineshape; this is likely due to magnetic susceptibility gradients

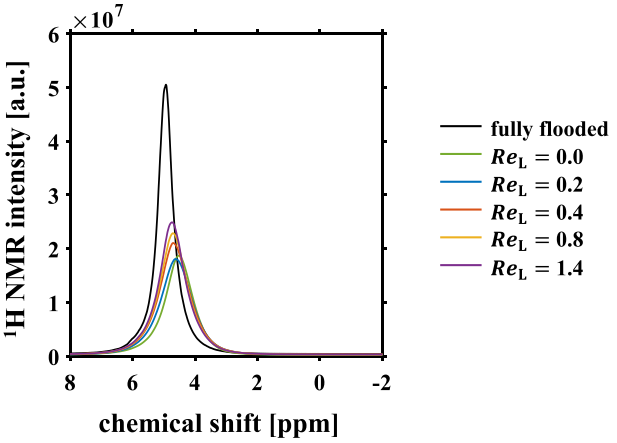

Fig. 3 ^{1}H NMR spectra obtained using a Hahn echo experiment. Spectra are referenced to the chemical shift of tetramethylsilane

at the gas-liquid interface. Note that all experimental and spectrometer parameters were kept the same for all experiments, and the echo time used (1 ms) is much shorter than the shortest T_2 relaxation time of liquid in the system ($T_2^{\text{intra}} \approx 150$ ms, Table 1). Therefore, the changes in signal intensity can be quantitatively interpreted as a change in the number of ^{1}H nuclei, and thus a change in the amount of liquid water, in the bed. The total signal intensity is quantified by integrating the spectra in Fig. 3, using integration limits from 2 to 7.5 ppm. The resulting signal intensity obtained by integration, I, normalized to the intensity of the spectra from the fully flooded bed, I_f, is reported in Table 2 for each flow condition studied. The normalized signal intensity, I/I_f, clearly increases with flow rate, indicating that liquid holdup indeed increases in the bed with flow rate.

To convert the signal intensity, I, into the liquid saturation in the bed, β, some consideration of the bed voidage, ϵ and pellet porosity, ϕ, is required. Recall that the liquid saturation, β, represents the fraction of inter-pellet void volume in the bed that is filled with liquid, and is required in the magnetization transport model to quantify ηk. The total signal intensity is written as:

Table 2 Hahn echo integrated signal intensity, I, normalized by the intensity from the fully flooded bed, I_f, at each flow condition studied

Re_L [−]	I/I_f[−]
0	0.60 ± 0.01
0.2	0.65 ± 0.01
0.4	0.73 ± 0.01
0.8	0.75 ± 0.01
1.4	0.79 ± 0.01

The error reported represents the standard deviation of three repeat measurements

$$I = \lambda \rho_{\text{spin}} V h, \tag{6}$$

where ρ_{spin} is the volumetric nuclear spin density of liquid water (number of ^{1}H nuclei per volume of water), V is the volume of the bed within the NMR active region, h is the total liquid holdup in the bed defined as the ratio of total liquid volume to the total bed volume (e.g. volume of the empty bed), and λ is the measured NMR signal per nuclear spin which is an empirical parameter dependent on the spectrometer sensitivity and pulse sequence details. Since all experiments were conducted at identical conditions and with identical spectrometer parameters, the normalized signal intensity is written:

$$\frac{I}{I_{\text{f}}} = \frac{h}{h_{\text{f}}}, \tag{7}$$

where h_{f} is the total liquid holdup in the fully flooded bed. Assuming that the intra-pellet liquid density is the same as the inter-pellet liquid density, and that the intra-pellet volume is fully liquid saturated, the holdup is written:

$$h = \epsilon\beta + (1-\epsilon)\phi. \tag{8}$$

Considering the average pore diameter of the silica pellets used here is 50 nm, both of these assumptions are reasonable as pores of this size do not substantially affect the liquid density [40], and due to capillarity the pores will be completely liquid saturated [41]. Combining Eqs. (7, 8) gives:

$$\frac{I}{I_{\text{f}}} = \frac{\epsilon\beta + (1-\epsilon)\phi}{\epsilon\beta_{\text{f}} + (1-\epsilon)\phi}, \tag{9}$$

where β_{f} is the liquid saturation in the fully flooded bed. Since care was taken to fully flood the bed, the liquid saturation in the fully flooded bed can be taken to be $\beta_{\text{f}} = 1$. Rearranging Eq. (9) gives:

$$\beta = \frac{\frac{I}{I_{\text{f}}}((1-\epsilon)\phi + \epsilon) - \phi(1-\epsilon)}{\epsilon}. \tag{10}$$

Equation (10) can therefore be used to quantify the bed liquid saturation, β, directly from the normalized signal intensities reported in Table 2.

Figure 4 shows the liquid saturation, β, calculated from the normalized signal intensity using Eq. (10), as a function of liquid Reynolds number, Re_{L}. In addition to the NMR calculated values, the liquid saturation predicted from the correlations of Larachi et al. [38] and Ellman et al. [39] are shown for comparison. From Fig. 4 it is seen that the liquid saturation increases with Reynolds number from $\beta = 0.16$ at $Re_{\text{L}} = 0$ to $\beta = 0.55$ at $Re_{\text{L}} = 1.4$. An increase in liquid saturation with liquid flow is predicted by both correlations. The measured value of liquid saturation falls between the value predicted by the two correlations for all conditions, except at $Re_{\text{L}} = 1.4$, where the measured value slightly exceeds the value predicted by the correlation of Ellman et al. [39]. At low Re_{L}, the measured value of β is in closer agreement with the correlation of Larachi et al. [38] whilst

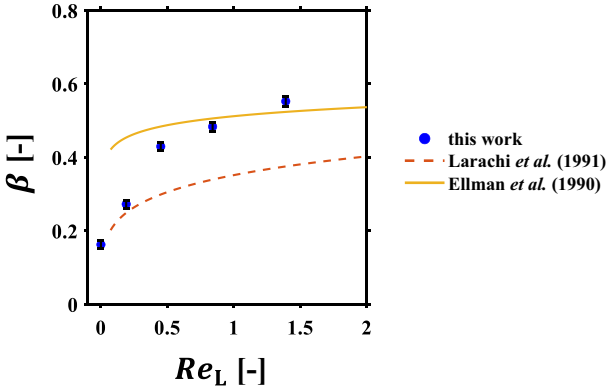

Fig. 4 Trickle bed liquid saturation, β, as a function of liquid phase Reynolds number, Re_L, calculated from the normalized signal intensity measurements using Eq. (10). In addition to the NMR measured values, the correlations of Larachi et al. [38] and Ellman et al. [39] are shown for comparison. Note that the original correlation of Ellman et al. [39] directly predicts the dynamic liquid saturation, β_{dyn}, rather than the total liquid saturation, β. To facilitate comparison, the value of β_{dyn} predicted from the correlation of Ellman et al. [39] was converted to the total liquid saturation, $\beta = \beta_{dyn} + \beta_{stat}$, by adding on the static liquid holdup measured experimentally using NMR at $Re_L = 0$

at higher values of Re_L the measured values show better agreement with the correlation of Ellman et al. [39].

The correlation of Larachi et al. [38] was developed using 1500 hydrodynamic measurements conducted using a wide range of fluids and flow conditions. However, the lowest liquid flow rate used in the development of the correlation of Larachi et al. [38] corresponds to $Re_L \approx 2$, thus this correlation is being extrapolated for the conditions studied herein. Further, Larachi et al. [38] only used non-porous glass pellets as the packing material, and did not use any data from beds with porous pellets in the development of the correlation. Whilst the correlation predicts the NMR measured values of liquid saturation well for $Re_L \leq 0.2$, values at higher Re_L are significantly underpredicted by the correlation. Lange et al. [42] also found the correlation of Larachi et al. [38] to underpredict the liquid saturation in trickle beds of porous pellets at $Re_L < 2$. The correlation of Ellman et al. [39] used over 5000 hydrodynamic experiments using a wide range of fluids, pellets, and flow conditions to develop their correlation. Notably, Ellman et al. [39] utilized both porous and non-porous pellets. The lowest liquid flow rate used in the correlation development corresponds to $Re_L \approx 0.8$, thus the correlation is being extrapolated for values below this. From Fig. 4 it is seen that the correlation of Ellman et al. [39] gives good agreement in the region where it is not being extrapolated, $Re_L \geq 0.8$. The agreement of the NMR measured values of liquid saturation with the correlation of Ellman et al. [39] where it is not being extrapolated, and thus can be expected to agree within a reasonable uncertainty, gives confidence in the NMR measurements of β. Taken together, the results of Fig. 4 demonstrate that the pellets and flow conditions used in the development of liquid holdup correlations are important, and further demonstrate that a simple NMR method can be used to accurately and non-invasively quantify the liquid saturation in trickle beds. These measurements of β can be

subsequently used in the magnetization transport model to quantify the mass transfer coefficient, ηk, from experimental $T_2 - T_2$ exchange measurements.

4.2 $T_2 - T_2$ exchange NMR and measurement of ηk

$T_2 - T_2$ exchange results for the fully flooded bed and for trickle flow over a range of Re_L at constant mixing time, $t_{mix} = 0.1$ s, are shown in Fig. 5. In the flooded bed, Fig. 5a shows two clear relaxation environments which, as in [18], can be attributed to intra- and inter-pellet fluid, with $T_2^{intra} \approx 0.15$ s and $T_2^{inter} \approx 1.2$ s. After the bed is drained and gas and liquid flow are introduced to the bed, the T_2 relaxation times decrease slightly for both the intra- and inter-pellet fluid. This decrease in (apparent) T_2 is most likely due to stronger internal magnetic gradients within the bed when gas is introduced to the bed due to magnetic susceptibility differences between gas and liquid. The decrease in the inter-pellet T_2 may also be due in part to decreased liquid saturation in the bed, whereby most of the liquid will exist in a film around the pellets and thus can more easily interact with the pellet surface. At higher liquid flow rates, $Re_L \geq 0.4$ (Fig. 5c–e), while the intra-pellet peak remains as a single peak at the same values of T_2 as those observed for lower values of Re_L (peak I), the inter-pellet T_2 peak is seen to split into two peaks, peaks II and III, with apparent T_2

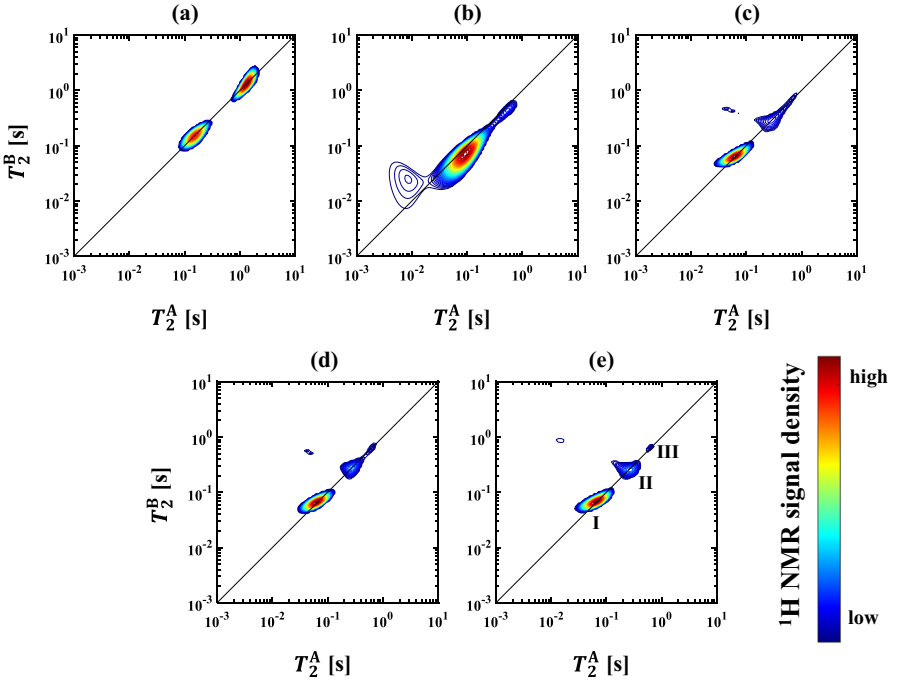

Fig. 5 2D T_2 distributions from $T_2 - T_2$ exchange experiments at mixing time $t_{mix} = 0.1$ s: **a** fully flooded bed; **b** $Re_L = 0.2$; **c** $Re_L = 0.4$; **d** $Re_L = 0.8$; **e** $Re_L = 1.4$. Note that trickle flow experiments (**b**–**e**) were conducted at constant gas flow $Re_G = 3.8$

values of approximately 0.4 s and 0.9 s. This splitting of the inter-pellet T_2 peak is likely due to an increase in liquid saturation in the bed with Re_L, as was observed in Fig. 4. At low liquid saturation, most of the inter-pellet liquid will exist as a thin film coating the pellet surface [31]. This film liquid may be more affected by magnetic gradients due to gas-liquid susceptibility differences, and further will have more interaction with the surface due to the limited film thickness, and thus shorter T_2 [43, 44]. As the liquid flow increases, thus resulting in a higher liquid saturation, some large pockets of liquid form that will not be as highly impacted by gas-liquid susceptibility differences and will have reduced interaction with the surface compared to liquid in the film. These results in the splitting of the inter-pellet T_2 peak into two separate peaks at $Re_L \geq 0.8$ (Fig. 5d, e). Peaks II and III are therefore assigned to inter-pellet liquid associated with liquid films on the pellets and large pockets of liquid in the inter-pellet space, respectively. A small cross peak is seen to form at flow rates $Re_L \geq 0.4$ (Fig. 5c–e). This is indicative of molecular exchange between the intra- and inter-pellet fluid. Because of the limited signal-to-noise ratio of the experiment, and small amount of exchange occurring at $t_{mix} = 0.1$ s, only one cross-peak is observed in Fig. 5c–e (rather than two symmetric cross-peaks). Investigation of the evolution of the cross-peaks as a function of t_{mix} can be used to directly probe the mass transport process occurring within the trickle bed.

The $T_2 - T_2$ exchange results acquired at $Re_L = 0.8$ are shown as a function of mixing time, t_{mix}, in Fig. 6. As t_{mix} increases, cross-peaks form and grow in intensity. At long t_{mix}, due to the lower SNR of the underlying measurements due to T_1 relaxation, the peaks become blurred and merge together somewhat, especially at $t_{mix} =$ 2.25 s (Fig. 6d). The inter-pellet water with the largest T_2 value (peak III, $T_2 \approx 0.9$ s), is seen to remain at all mixing times and not split into cross-peaks for the mixing times studied here, whereas the inter-pellet water with the intermediate T_2 value (peak II, $T_2 \approx 0.4$–0.5 s), forms substantial cross-peaks with the intra-pellet water due to molecular exchange. This is largely consistent with the previously discussed interpretation that the longest T_2 value (peak III) is attributable to large pockets of water, which will be the slowest to exchange with the intra-pellet liquid (peak I). To quantify the cross-peak intensity, I_{XP}, the cross-peak regions in the 2D T_2 distributions were integrated as described in [18]. To account for the error incurred when selecting the integration regions, which has previously been shown to be the largest source of error when quantifying I_{XP} [45], the integration bounds were increased/decreased as shown by the red shading in Fig. 6c. Similar integration bounds to that shown in Fig. 6c were used for all values of t_{mix}.

The cross-peak intensity, I_{XP}, normalized by the total peak intensity in the 2D T_2 distribution, I_{TP}, is shown as a function of mixing time in Fig. 7, along with the best fit of the trickle bed magnetization transport model (Eqs. (2–4)) to the experimental data for each flow condition studied. The resulting mass transfer coefficients, ηk, extracted from the best fit of the model are reported in Table 3. As expected, and as was observed in [18] for single phase flow, the cross-peak intensity increases faster at larger Re_L, indicative of faster mass transfer between the intra- and inter-pellet phase. This is captured by the magnetization transport model, which reports an increase in ηk as Re_L increases (Table 3). Considering that only a single fitting parameter is used in the model (ηk), the model fits the experimental data in Fig. 7

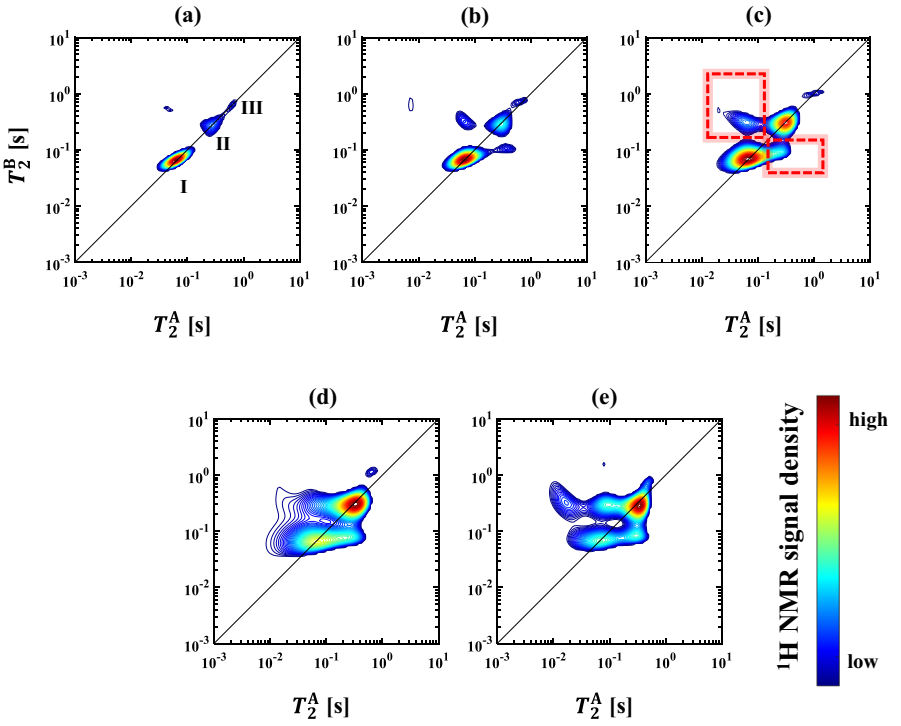

Fig. 6 2D T_2 distributions from $T_2 - T_2$ exchange experiments at $Re_L = 0.8$ over a range of mixing times, t_{mix}: **a** $t_{mix} = 0.1$ s; **b** $t_{mix} = 0.75$ s; **c** $t_{mix} = 1.5$ s; **d** $t_{mix} = 2.25$ s; **e** $t_{mix} = 3.0$ s. Note that all trickle flow experiments were conducted at constant gas flow $Re_G = 3.8$. The cross-peak integration regions are shown by the dashed red lines in panel (**c**). The shaded red region represents the uncertainty in the integration region used to estimate the error in the cross-peak intensity, I_{XP}

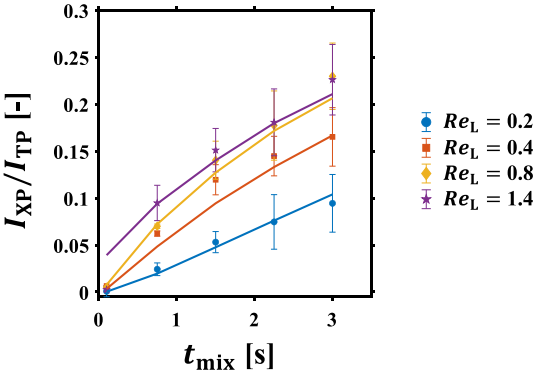

Fig. 7 $T_2 - T_2$ cross peak evolution profiles, $I_{XP}/I_{TP}(t_{mix})$, as obtained from the experimental NMR data (points) and the best fit of the trickle bed magnetization transport model to the data (solid lines) at each flow condition. Error bars represent the variation of I_{XP}/I_{TP} when the integration bounds were varied

very well. The good agreement between model and experimental cross-peak profiles demonstrates that the magnetization transport model developed in [18] can indeed be successfully extended to trickle bed systems, despite the more complicated

Table 3 Mass transfer coefficients, ηk, extracted from the fit of the magnetization transport model to the experimental $T_2 - T_2$ exchange data

Re_L [−]	$\eta k \times 10^6$ [m s^{-1}]
0.2	2.5 ± 1
0.4	8.2 ± 3
0.8	23 ± 10
1.4	26 ± 11

Error bars represent the 95% parameter confidence interval for ηk obtained from non-linear least squares regression

multiphase flow physics. The resulting mass transfer coefficients can subsequently be compared to existing literature correlations to assess how the $T_2 - T_2$ NMR technique compares to established measurements of mass transfer.

4.3 Comparison Of Dimensionless Mass Transfer Coefficients With Existing Correlations

The mass transfer coefficients measured using the $T_2 - T_2$ exchange NMR method in this work are compared to four literature correlations for the mass transfer coefficient in trickle beds in Fig. 8. The mass transfer coefficients are presented in dimensionless form, $\eta Sh = \eta \frac{k d_p}{D_L}$, to facilitate comparison with the mass transfer correlations from the literature, which are typically in dimensionless form. Note that D_L is the molecular diffusivity of the inter-pellet liquid phase, taken here as $D_L = 2.2 \times 10^{-9}$ m^2 s^{-1} [46]. The correlations compared here, as summarized in Table 4, were developed using a variety of experimental techniques and pellet materials. From Fig. 8 it is seen that the mass transfer coefficients measured in this work using relaxation exchange NMR fall within the range given by the correlations. This gives

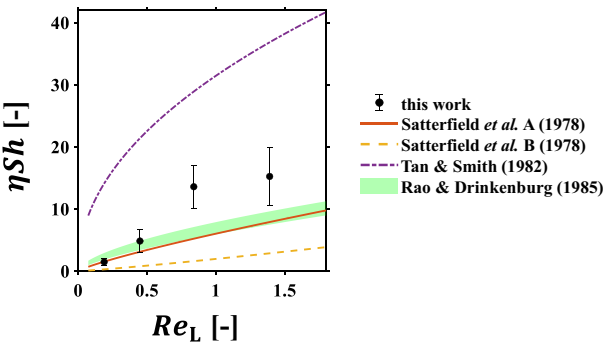

Fig. 8 Dimensionless mass transfer coefficient, ηSh, as a function of liquid Reynolds number, Re_L. The results from $T_2 - T_2$ exchange NMR measurements are plotted along with the correlations of Satterfield et al. [48], Tan and Smith [17], and Rao and Drinkenburg [47] for comparison. Note that the correlation of Rao and Drinkenburg [47] requires the liquid saturation, β. To evaluate the correlation of Rao and Drinkenburg [47], the liquid saturation correlations of Larachi et al. [38] and Ellman et al. [39] were both used, and the resulting range of ηSh is presented by the shaded green region

Table 4 Correlations for ηSh in trickle beds obtained using a variety of experimental methods

Satterfield et al. A [48]	$\eta Sh = 0.815\ Re_L^{0.822} Sc^{1/3}$; $1.5 < Re_L < 196$; $0 < Re_G < 433$ Method: dissolution Fluids: water, N_2, He, Ar Packing: non-porous benzoic acid cylinders
Satterfield et al. B [48]	$\eta Sh = 0.266\ Re_L^{1.147} Sc^{1/3}$; $Re_L < 20$; $Re_G = 0$ Method: dissolution Fluids: water, aqueous solutions of glycerol and surfactants Packing: non-porous benzoic acid cylinders
Tan and Smith [17]	$\eta Sh = 4.25\ Re_L^{0.48} Sc^{1/3}$; $0.88 < Re_L < 34.5$; $0.1 < Re_G < 2.7$ Method: dynamic adsorption Fluids: aqueous benzaldehyde, He Packing: porous activated carbon particles
Rao and Drinkenburg [47]	$\eta Sh = 0.24\left(Re_L/\beta\right)^{0.75} Sc^{1/3}$; $70 < Re_L < 250$; $11 < Re_G < 385$ Method: electrochemical Fluids: aqueous electrolyte solution, air Packing: non-porous glass and nickel electrode cylinders

Note that the Schmidt number is defined as $Sc = \frac{\mu_L}{\rho D_L}$, where D_L is the molecular diffusion coefficient of the (inter-pellet) liquid phase

confidence that the NMR relaxation exchange technique developed in this work can be successfully employed to measure mass transfer coefficients within trickle beds. The correlation of Rao & Drinkenburg [47] and correlation A from Satterfield et al. [48] show the best agreement with the NMR measurements. However, at $Re_L \geq 0.8$, these correlations somewhat underpredict the measured value of ηk. Correlation B from Satterfield et al. [48] is seen to underpredict the measurements, while the correlation of Tan and Smith [17] is seen to overpredict the measurements at all Re_L studied.

The correlation of Tan and Smith [17] has previously been reported to overpredict *operando* measurements of the mass transfer coefficient in a trickle bed [4]. This overprediction was attributed to the manner in which Tan and Smith introduced liquid into the bed, whereby the liquid was fed in large capillary tubes which may have caused forced pulsing flow in the bed. Correlation B from Satterfield et al. [48] used data collected with zero gas flow, $Re_G = 0$, and as such does not account for any effects that gas flow rate causes on the liquid mass transfer. Given that Saroha [49] observed a weak increase in k with increasing gas flow rate in the trickle flow regime, not accounting for the effect of gas flow may be the reason that correlation B from Satterfield et al. [48] underpredicts the values of ηk measured in this work. Correlation A from Satterfield et al. [48] and the correlation of Rao and Drinkenburg [47] were developed using the dissolution and electrochemical method, respectively. Further, both were developed from data collected at a higher liquid flow rates than those studied here (Table 4), and using non-porous pellets. Despite these differences, both of the aforementioned correlations show good agreement with the NMR measured values of ηk at $Re_L \leq 0.4$, but at $Re_L \geq 0.8$ these correlations underpredict the measured value of ηk. Since ηk increases with Re_L, it seems unlikely that this underprediction is caused by extrapolating the correlation to low Re_L. Rather, the underprediction is more likely caused by the pellet porosity and/or the pellet wettability.

The porosity and wettability of pellets has previously been observed to affect pellet wetting efficiency, pressure drop and flow texture in trickle beds [13, 31, 50]. Specifically, Baussaron et al. [14] have observed that η depends on the liquid-solid interaction strength at low liquid flow rates, comparable to those studied here. Thus, the exclusive use of non-porous pellets to develop Correlation A from Satterfield et al. [48] and the correlation of Rao and Drinkenburg [47], may be the cause of the underprediction of the measured value of ηk at $Re_L \geq 0.8$. In further support of this suggestion, Tan and Smith [17] used porous pellets in the development of their correlation, which subsequently predicts much higher values of ηk than either of the correlations developed using non-porous pellets. Although the larger values predicted by Tan and Smith [17] may be due in part to the previously mentioned issue of liquid pulsing, it is also possible that this is partially due to the use of porous as opposed to non-porous pellets. Taken together, the results reported in Fig. 8 suggest that the NMR relaxation exchange method can be used to quantitatively measure the mass transfer coefficient, ηk, in trickle beds at low liquid flow rates. Comparison with correlations demonstrates the importance of considering the assumptions, flow conditions and pellet materials used to develop mass transport correlations when selecting an appropriate correlation for use in designing or scaling up a trickle bed process. Whilst the measurements conducted in this work were conducted using a high-field magnet, in principle the mass transfer coefficient could be measured using a portable low-field magnet. In a low-field implementation of this method, it may not be possible to measure the liquid saturation, β, using the Hahn echo procedure reported herein which relies on chemical shift difference between inter- and intra-pellet liquid, and the use of correlations for β may be required. However, the relaxation exchange measurements could likely be directly conducted on a low-field magnet, as demonstrated by Olaru et al.[30], and subsequently used to obtain the mass transfer coefficient. A low-field implementation of the present technique would significantly improve the accessibility of this method for use by chemical engineering practitioners.

5 Conclusions

In this work, the $T_2 - T_2$ relaxation exchange NMR method for measuring the mass transfer coefficient developed in [18] was successfully extended to quantify the liquid-solid mass transfer coefficient in a trickle bed of porous silica pellets. To achieve this, the magnetization transport model derived for single-phase flow in a packed bed was adapted to account for the partial surface wetting and partial liquid saturation within a trickle bed. To directly measure the molecular exchange between intra- and inter-pellet liquid in the bed, $T_2 - T_2$ exchange experiments were conducted over a range of liquid flow rates $0.2 \leq Re_L \leq 1.4$, at a constant gas flow rate $Re_G = 3.8$. The cross-peak intensity, I_{XP}, from the $T_2 - T_2$ exchange experiments, indicative of molecular exchange, increased with both exchange time, t_{mix}, and liquid flow rate. The magnetization transport model was found to fit the cross-peak evolution data accurately using the mass transfer coefficient as the sole fitting parameter. The resulting values of the mass transfer coefficient were compared to several commonly used literature correlations, with the values measured using the NMR method falling within the range predicted by the

correlations. Comparison of the mass transfer coefficient measured by NMR with the correlations demonstrates the importance of considering the flow conditions and pellets used to develop mass transfer correlations when selecting a correlation to use for a specific bed. Importantly, the method developed here can be utilized on other pellet geometries and support materials of commercial relevance. As such, this method can be used in the future for the screening and optimization of catalyst pellets and reactor operating conditions for optimal mass transport properties.

Acknowledgements The authors thank Shell Global Solutions International B.V. for funding supporting this work. SVE thanks the Sir Winston Churchill Society of Edmonton and the Natural Sciences and Engineering Research Council of Canada for additional financial support. QZ thanks the IChemE Andrew Fellowship for additional financial support. For the purpose of open access, the authors have applied a Creative Commons Attribution (CC BY) licence to any Author Accepted Manuscript version arising from this submission.

Authors' contributions SVE, AJS, MDM and LFG contributed to the study's conception and design. SVE and NA setup the trickle bed rig and conducted the experiments. SVE and QZ conducted the data analysis and modelling. SVE wrote the first draft of the manuscript. SVE, AJS and LFG edited and revised the manuscript. All authors read and approved the final version of the manuscript.

Funding The authors thank Shell Global Solutions International B.V. for funding supporting this work. SVE thanks the Sir Winston Churchill Society of Edmonton and the Natural Sciences and Engineering Research Council of Canada for additional financial support. QZ thanks the IChemE Andrew Fellowship for additional financial support.

Data availability The data that support the findings of this study are available from the corresponding author upon reasonable request.

Declarations

Ethical approval Not applicable.

Conflict of interest The authors have no relevant financial or non-financial interests to disclose.

References

1. M.H. Al-Dahhan, F. Larachi, M.P. Dudukovic, A. Laurent, Ind. Eng. Chem. Res. **36**, 3292 (1997)
2. M. P. Dudukovic, Ž. V. Kuzeljevic, and D. P. Combest, in *Ullmann's Encycl. Ind. Chem.* (Wiley-VCH Verlag GmbH & Co. KGaA, Weinheim, Germany, 2014), pp. 1–40.
3. A. Gianetto, V. Specchia, Chem. Eng. Sci. **47**, 3197 (1992)
4. Q. Zheng, F.J. Russo-Abegao, A.J. Sederman, L.F. Gladden, Chem. Eng. Sci. **171**, 614 (2017)
5. I. Stamatiou, F.L. Muller, Chem. Eng. J. **377**, 119808 (2019)
6. W.E. Stewart, E.N. Lightfoot, D.H. Hunt, Z. Eng, C.N. Satterfield, A.A. Pelossof, T.K. Sherwood, AIChE J. **15**, 226 (1969)

7. B.W. Gamson, G. Thodos, O.A. Hougen, Trans. Am. Inst. Chem. Eng. **39**, 495–516 (1943)
8. E.J. Wilson, C.J. Geankoplis, Ind. Eng. Chem. Fundam. **5**, 9 (1966)
9. J.E. Williamson, K.E. Bazaire, C.J. Geankoplis, Ind. Eng. Chem. Fundam. **2**, 126 (1963)
10. A.J. Karabelas, T.H. Wegner, T.J. Hanratty, Chem. Eng. Sci. **26**, 1581 (1971)
11. F. Coeuret, Electrochim. Acta **21**, 185 (1976)
12. M. Yoshikawa, K. Iwai, S. Goto, H. Teshima, J. Chem. Eng. Japan **14**, 444 (1981)
13. R. Maiti, A. Atta, K.D.P. Nigam, Ind. Eng. Chem. Res. **47**, 8126 (2008)
14. L. Baussaron, C. Julcour-Lebigue, C. Boyer, A.M. Wilhelm, H. Delmas, Chem. Eng. Sci. **62**, 7020 (2007)
15. S. Morlta, J.M. Smith, Ind. Eng. Chem. Fundam. **17**, 113 (1978)
16. A.J. van Houwelingen, W. Nicol, AIChE J. **57**, 1310 (2011)
17. C.S. Tan, J.M. Smith, AIChE J. **28**, 190 (1982)
18. S.V. Elgersma, A.J. Sederman, M.D. Mantle, L.F. Gladden, Chem. Eng. Sci. **248**, 117229 (2022)
19. J.H. Lee, C. Labadie, C.S. Springer, G.S. Harbison, J.H. Lee, C. Labadie, C.S. Springer, G.S. Harbison, J. Am. Chem. Soc. **115**, 7761 (1993)
20. K.M. Song, J. Mitchell, H. Jaffel, L.F. Gladden, J. Phys. D. Appl. Phys. **45**, 105302 (2012)
21. J.J. Chen, J.A. Mason, E.D. Bloch, D. Gygi, J.R. Long, J.A. Reimer, Microporous Mesoporous Mater. **205**, 65 (2015)
22. M.N. d'Eurydice, E.T. Montrazi, C.A. Fortulan, T.J. Bonagamba, J. Chem. Phys. **144**, 204201 (2016)
23. C. Terenzi, A.J. Sederman, M.D. Mantle, L.F. Gladden, J. Magn. Reson. **299**, 101 (2019)
24. J.D. Griffith, J. Mitchell, A.E. Bayly, M.L. Johns, J. Phys. Chem. B **113**, 7156 (2009)
25. J. Kolz, Y. Yarovoy, J. Mitchell, M.L. Johns, L.F. Gladden, Polymer **51**, 4103 (2010)
26. K. E. Washburn, C. H. Arns, and P. T. Callaghan, Phys. Rev. E Stat. Nonlinear, Soft Matter Phys. **77**, (2008).
27. S.E. Mailhiot, F. Zong, J.E. Maneval, R.K. June, P. Galvosas, J.D. Seymour, J. Magn. Reson. **287**, 82 (2018)
28. J. Cox, P.J. McDonald, B.A. Gardiner, Holzforschung **64**, 259 (2010)
29. M. van Landeghem, A. Haber, J.-B. d'Espinose de Lacaillerie, B. Blümich, Concepts Magn. Reson. Part A **36A**, 153 (2010)
30. A.M. Olaru, J. Kowalski, V. Sethi, B. Blümich, J. Magn. Reson. **220**, 32 (2012)
31. L. Baussaron, C. Julcour-Lebigue, A.M. Wilhelm, H. Delmas, C. Boyer, AIChE J. **53**, 1850 (2007)
32. L. Díaz Anadón, Transient Hydrodynamics and Reaction in Trickle-Bed Reactors Using NMR and MRI, University of Cambridge, 2007.
33. J. Levec, A.E. Sáez, R.G. Carbonell, AIChE J. **32**, 369 (1986)
34. W. Van Der Merwe, W. Nicol, Ind. Eng. Chem. Res. **44**, 9446 (2005)
35. L. Venkataramanan, Y.Q. Song, M.D. Hürlimann, IEEE Trans. Signal Process. **50**, 1017 (2002)
36. E.A. Foumeny, F. Benyahia, Heat Recover. Syst. CHP **11**, 127 (1991)
37. A. Attou, C. Boyer, G. Ferschneider, Chem. Eng. Sci. **54**, 785 (1999)
38. F. Larachi, A. Laurent, N. Midoux, G. Wild, Chem. Eng. Sci. **46**, 1233 (1991)
39. M.J. Ellman, N. Midoux, G. Wild, A. Laurent, J.C. Charpentier, Chem. Eng. Sci. **45**, 1677 (1990)
40. L. Travalloni, M. Castier, F.W. Tavares, S.I. Sandler, J. Supercrit. Fluids **55**, 455 (2010)
41. J.G. Schwartz, E. Weger, M.P. Duduković, AIChE J. **22**, 894 (1976)
42. R. Lange, M. Schubert, T. Bauer, Ind. Eng. Chem. Res. **44**, 6504 (2005)
43. C. I. Robertson, Characterising Adsorption and Mass Transfer in Porous Media, University of Cambridge, 2018.
44. A. R. Klotz, Towards an Understanding of Mass Transfer and Hydrodynamics in Packed Bed Reactors Using Nuclear Magnetic Resonance, University of Cambridge, 2019.
45. J. Mitchell, J.D. Griffith, J.H.P. Collins, A.J. Sederman, L.F. Gladden, M.L. Johns, J. Chem. Phys. **127**, 204201 (2007)
46. M. Holz, S.R. Heil, A. Sacco, Phys. Chem. Chem. Phys. **2**, 4740 (2000)
47. V.G. Rao, A.A.H. Drinkenburg, AIChE J. **31**, 1059 (1985)
48. C.N. Satterfield, M.W. Van Eek, G.S. Bliss, AIChE J. **24**, 709 (1978)
49. A.K. Saroha, Chem. Eng. Res. Des. **88**, 744 (2010)
50. P.V. Ravindra, D.P. Rao, M.S. Rao, Ind. Eng. Chem. Res. **36**, 5133 (1997)